Libyan Journal of Applied and Contemporary Sciences
ISSN
E: 3136-3709
L: 3136-3695
Vol 1: No 2

The antibacterial Activity of Aspergillus niger-Mediated TiO_2 Nanoparticles against Clinical Pseudomonas aeruginosa Isolates

Hanan Hamed

Department of Biology, College of Science, University of Anbar, Anbar, Iraq

**Email corresponding author's: hanan.hamid@uoanbar.edu.iq*

Received: 13/8/2026 Accepted: 16/10/2026 Published: 30/10/2026

Abstract

Pseudomonas aeruginosa is a multidrug resistant bacterium, which is a major therapeutic challenge. In this study, cell-free filtrate of *Aspergillus niger* was used as a source to prepare the TiO_2 nanoparticles and tested against 9 clinical *P. aeruginosa* isolates. X-ray diffraction (XRD), FTIR, dynamic light scattering (DLS), zeta-potential analysis, STEM and SEM were used for physicochemical characterization. The XRD profile exhibited a broad diffuse reflection around 23.5° (2θ), but not enough reflections were resolved to distinguish anatase and rutile. DLS results gave a Z-average hydrodynamic diameter of 28.38 nm (PdI 0.383), but intensity peaks of 27.70 and 147.8 nm were obtained which are not directly comparable to dry-state dimensions measured by SEM. The reported zeta potential was +17.1 mV which indicates minimal electrostatic stabilization during the reported conditions. After exposure to the nanoparticles the growth of all of the nine isolates was inhibited, as demonstrated by the presence of measurable inhibition zones (12–20 mm) and MIC ranged from 50 to 100 µg/mL. The results showed no growth of subculture at tested concentration for isolates 1, 2 and 5 while the bactericidal endpoints were not achieved for other isolates. These findings in-vitro are indications of further investigation of this preparation as a bactericidal, but don't constitute a universal bactericidal effect, mechanism of action or clinical efficacy.

Keyword : *Green synthesis; Aspergillus niger; titanium dioxide nanoparticles; multidrug resistance; Pseudomonas aeruginosa; minimum inhibitory concentration; minimum bactericidal concentration .*

Doi : https://doi.org/10.64943/ljacs.2026.010217

Copyright © 2026 Author(s) ; Published by Libyan Journal of Applied and Contemporary Sciences
This is an open access article licensed under CC BY: (https://creativecommons.org/licenses/by/4.0)

INTRODUCTION

AMR is no longer confined to the laboratory setting, but is one of the biggest public health problems of the twenty-first century. Systematic global studies show that almost five million deaths per year can be caused by bacterial AMR, whether directly or in association, and future forecasts predict that this number may increase significantly before mid-century if the present trends of resistance continue (1), (2). In light of this, the 2024 Bacterial Priority Pathogens List published by the WHO once again included carbapenem resistant *Pseudomonas aeruginosa* in the list of critical pathogens (1,3). *Pseudomonas aeruginosa* is an opportunistic Gram-negative bacteria which is the cause of most cases of nosocomial pneumonia, bacteremia, wound infection, and catheter-related infection and has been known for its resistance to virtually all clinically available antibiotics (4).Carbapenems like meropenem have traditionally been used as a last resort for treatment of multidrug-resistant (MDR) Gram-negative infections, but carbapenem-resistant *P. aeruginosa* (CRPA) has been reported with incidences ranging from below 3% to 59%, through various mechanisms like porin mutation, overexpression of efflux systems, AmpC production, and, increasingly, development of transferable carbapenemases (5,6,7,8). Clinical studies indicate that CRPA BSI is linked to a significantly greater mortality compared to carbapenem susceptible BSI (9), highlighting the need for the identification of compounds which remain effective against these strain.

Nanomaterials with antimicrobial properties have been found to be among the most studied alternatives to traditional antibiotics because many of these nanomaterials use physical mechanisms of action, such as membrane disruption, ion release, and production of reactive oxygen species (ROS), that are not susceptible to the mechanisms of classical antibiotic resistance like point mutations, efflux pumps, and

hydrolytic enzymes (10,11,12). The metal-oxide nanomaterials are promising because they are manufactured from a widely available metal, are chemically stable, have a long history of use in various regulatory environments including cosmetics and sunscreens, food contact materials, and biomedical applications, and are already used in clinical settings (13,14,15). TiO_2NPs possess natural antimicrobial properties that can be significantly improved by illumination of these particles with UV and visible light due to their photocatalytic ability to produce hydroxyl radicals (OH), superoxide anions (O_2^-), and other ROS, which are able to oxidize membrane phospholipids, proteins, and nucleic acids, leading to disruption of cell-envelope integrity (16). Other than enzymatic action, this method of killing does not show any target specificity and that Gram-negative bacteria that are resistant to all of the commonly used β-lactams, fluoroquinolones and aminoglycosides have been found to be susceptible to TiO_2 NPs as well as other nanomaterials (17,16,4)

The chemical synthesis techniques used to synthesize TiO_2 NPs, such as sol-gel, hydrothermal, and chemical vapor deposition, involve the use of organic solvents, surfactants, and/or high temperatures during calcination, which raises costs and can result in environmental damage, and generate effluents (18). Biological synthesis methods or green chemistry synthesis methods using bacteria, fungi, yeast, algae and plant extracts are one of the processes that have been conducted with an energy efficient energy that are reduced by enzymes and secondary metabolites in the process of reducing metal ions and capping the resulting metal nanoparticles (19, 20, 21). The filamentous fungi are especially interesting because they produce a lot of extracellular reductases and oxidoreductases, and are also very resistant to the stress caused by metal ions in their culture process, especially the genus *Aspergillus*, which has been used in the mycosynthesis of various nanomaterials such as nanosilver, nanogold, zinc oxide, copper oxide, and selenium-based nanoparticles, with confirmed antibacterial, antibiofilm, and anticancer activity (22, 23, 24, 1). In particular, *Aspergillus niger* was repeatedly demonstrated to be able to synthesize metal or metal oxide nanoparticles extracellularly using the bioreduction of nitrate with nitrate reductase and a protein/polysaccharide capping process (23, 24, 25). However, the use of A. niger in the biogenesis of TiO2 NPs has relatively gone unnoticed compared to TiO2 production by plants or bacteria (22, 26, 27, 28). The antibacterial activity cannot be dissociated from the evaluation of efficacy, and the structure, colloidal stability and surface properties of the biologically synthesized TiO2 NPs, namely the type of biomolecular layer coating the surface of these NPs, their crystallinity and crystal phase (anatase versus rutile) and their hydrodynamic size and surface charge, are known to control the antibacterial activity (29, 30, 31). Generally, the TiO_2NPs with the anatase phase or those that are nano or amorphous in form have a high surface-to-volume ratio and are more effective in ROS production and antibacterial effects than the bulk or highly crystalline rutile form of TiO_2 (32). The biomolecular coating generated during the green synthesis using fungi can also affect the interaction of bacteria nanoparticles (19, 20, 21), detectable by amide I/II band in the FTIR spectrum. On this premise, the current work aims at (i) mycosynthesizing the TiO_2 NPs using cell-free filtrate of *A. niger* (ii) characterizing the synthesized nanomaterial by XRD, FTIR, DLS, zeta potential, STEM and FE-SEM; and (iii) testing its antibacterial efficacy by disc diffusion, broth microdilution MIC and subculture-validated MBC against nine *P. aeruginosa* clinical isolates, where compared to standard antipseudomonal antibiotics. Considering that the potential for nanoparticle antibiotic conjugates against MDR Gram-negative bacteria has been reported (33, 34, 35, 36, 37), and the proven efficacy of metallic and metal oxide nanoparticles in inhibiting biofilm formation in P. aeruginosa (38, 39, 40, 41, 42), we extend our discussion here to the translation of our findings into treatment of XDR *P. aeruginosa*.

MATERIALS AND METHODS

Fungal strain, culture conditions and preparation of the cell-free filtrate

Potato Dextrose Broth (PDB) was used as the nutrient medium for the culture of *Aspergillus niger*. All inoculated flasks of *A. niger* were grown for 3–4 days at 200 rpm and 28–30 °C in a rotary shaker for good development of mycelial growth. The fungal biomass after the incubation period was filtered out with a special filtration system and pelleted by centrifugation. The filtered fluid containing the enzymes

and other metabolites produced in the subsequent bioreduction process was retained for further use (43).

Biosynthesis of TiO2 nanoparticles

The cell-free filtrate obtained from the fungus was added to an aqueous titanium precursor solution in a ratio of 1:10 (v/v) as reported. The pH of the reaction was adjusted to about 9 and the mixture was kept for 24–96 hours. During the reaction, a visible colour change was seen but this does not provide identity of the nanoparticles or the chemical composition. The material obtained was centrifuged, washed in distilled water and ethanol and dried. The identity of the precursor, provisionally identified as $Ti(NO_2)$ in Figure 1, was not determined from the provided record, and would need to be confirmed from the original laboratory record prior to publication. No other identity is taken on.



Figure 1. Change in color of the fungal filtrate due to reaction with $Ti(NO_3)_2$ precursor solution for 72 hours.

Physicochemical characterization

X-ray diffraction (XRD) was obtained in the range of 2θ between 7 and 100°. The phase identification was judged on the presence or not of the Bragg reflections that are diagnostic for the phase; Scherrer equation cannot be used on an unresolved diffuse halo. FTIR was acquired over 399–4000 cm^{-1}. DLS, electrophoretic mobility measurements were carried out in aqueous dispersion at 25 °C while STEM and FE-SEM were used for qualitative evaluation of the morphology. The calibrated image analysis of multiple particles and fields was required to provide quantitative particle-size statistics, which were unavailable to perform independent reanalysis.

Antibacterial susceptibility testing by agar diffusion

Nine clinical P. aeruginosa isolates (1) were used in this study.The CAZ (30 µg), PRL (100 µg), MEM (10 µg), CIP (5 µg), CN (10 µg), ATM (30 µg) and the nanoparticle preparation were evaluated using the reported agar disc/well diffusion protocol. The size of the inhibition zones were measured at 24 hours after incubation at 37 °C and the suspensions were adjusted to 0.5 McFarland. Available manuscript does not report the loading of the nanoparticles per well/disc nor validated susceptibility breakpoints, therefore the zones of the nanoparticles are reported as inhibition measurements, not clinical susceptible/resistant zones.

Determination of the minimum inhibitory concentration (MIC) and minimum bactericidal concentration (MBC)

The reported MIC testing was performed by broth dilution of the nanoparticles in Brain Heart Infusion (BHI) medium and meropenem was taken from a stock solution of 1000 µg/mL. Cultures were grown for 24 h at 37 °C, and visually estimated for turbidity and measured by OD600. Micro plate-based method is not documented as per original protocol which describes macro dilution. The reported MICs are not corrected for possible influence of nanoparticle suspensions on optical readings; therefore, the reported values should be interpreted with caution unless concentration matched nanoparticle-only blanks are not available. 100 µL of subcultures were taken from the selected tubes (at or above MIC) and grown on BHI agar, and were then assessed after 24 h for MBC. No growth in the aliquot cultured is not a verified 99.9% reduction in viable counts, but rather a no growth subculture endpoint.

Statistical analysis

Triplicate antibacterial susceptibility testing has been reported in the manuscript. The results of the descriptive tests are presented as inhibition-zone diameter and reported endpoint of MIC/MBC. No inferential significance tests are claimed for. The MIC values for nanoparticles and meropenem are different sample sizes and observations. The microscopy sizes listed are single measurements based on images and not mean values of a population.Replicate measurements of the isolate level are not provided and so the reported replicate testing cannot be independently summarized as mean ± SD. The values in Table 1 are presented as stated and no p-values, confidence intervals or claims of significance are implied.

RESULTS AND DISCUSSION

X-ray diffraction (XRD) analysis

The XRD profile available (Figure 2) is broad and diffuse at 2θ ~ 23.5° and has a weak feature in the vicinity of the 30° value. Both of these features are not well developed enough to index unambiguously to anatase, rutile or brookite. No special Miller indices or crystallite size is given. For rigorous phase identification, a background-corrected diffractogram from the instrument, instrumental parameters and reference diffraction patterns are needed. The diffuse scattering agrees with only partial long range order and does not provide any information on the chemical identity or crystalline phase of TiO2. There is no direct linking between SEM particle size and DLS hydrodynamic diameter to define crystallinity independent of each other. As such, these XRD data do not allow for an inference of any photocatalytic mechanism or mechanism involving the production of reactive-oxygen-species specific for anatase.

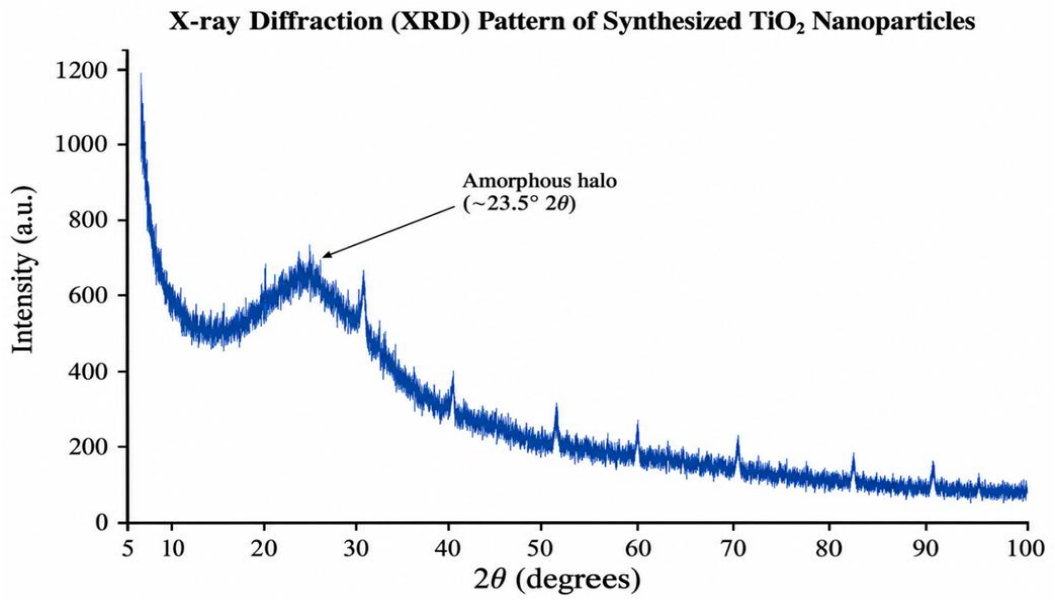


Figure 2. XRD pattern of the as-prepared nanoparticle sample showing a broad diffuse feature near 2θ = 23.5° and a weak shoulder near 30°. Neither feature is assigned to a specific TiO_2 crystal plane because diagnostic, resolved reflections are absent. Phase identification and peak-indexed redrawing require the original instrument data and reference-pattern matching.

Fourier-transform infrared (FTIR) spectroscopy

The FTIR spectrum contains bands near 3090, 1605, 1557, 1402, 1257, 1084 and below 600 cm¹. The low wavenumber region has absorptions that are compatible with metal oxygen vibrations, and the amide-region and hydroxyl-region absorptions indicate the presence of organic residues from the fungal filtrate as shown in the (figure 3) . These assignments are tentative but can only be made based on the FTIR spectra; confirmation of the composition of TiO2 by EDX or XPS analysis is still required, and there are no definitive conclusions regarding a specific bonding mechanism between the surface and proteins yet. The designation TiO2 was preferred to the assignment of a definitive diffraction-phase which because of the absence of elemental composition was not independently established, thus some care must be taken in interpreting the content of the designation (24,37,47).

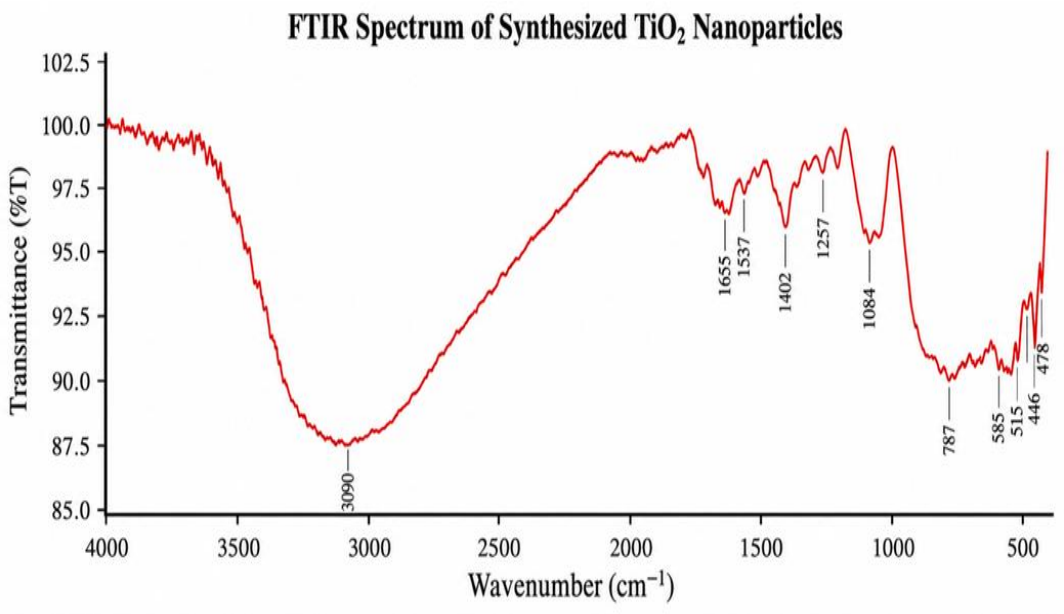


Figure 3. FTIR spectrum of the reported nanoparticle preparation. Bands in the low-wavenumber region are consistent with metal–oxygen vibrations, while amide- and hydroxyl-region bands may reflect residual fungal-derived organic compounds; these assignments do not independently establish surface-coating composition.

Dynamic light scattering (DLS) particle size analysis

A reported Z-average hydrodynamic diameter of 28.38 nm and PdI = 0.383 were obtained using DLS (Figure 4) . The modes in the intensity distribution were around 27.70 nm with 71.5% of the intensity and around 147.8 nm with 28.5% of the intensity, while the mode of the transformed number distribution was around 11.20 nm. The number distribution is not an independent particle count and the intensities are not percentages of particles. There is a relatively wide PdI and secondary intensity mode suggesting a degree of heterogeneity and aggregation. It is not possible to directly compare DLS to dry-particle SEM dimensions, and the reported Z-average should be compared to the instrument export data from the original.

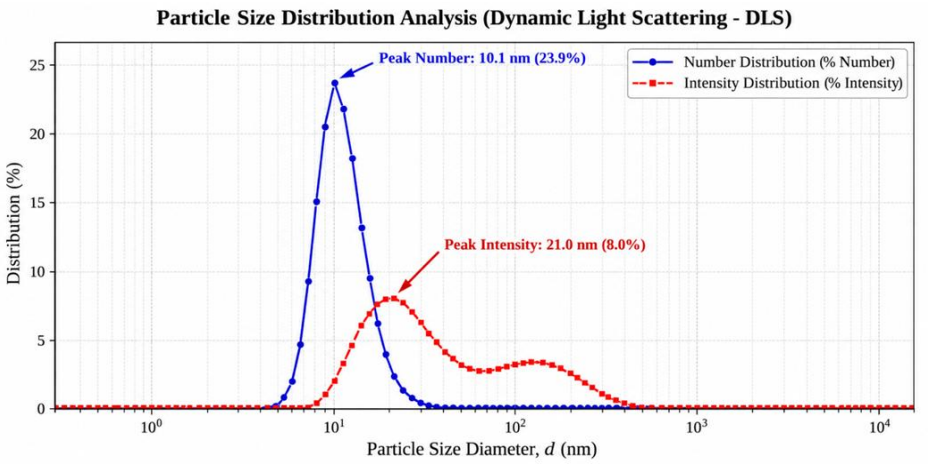


Figure 4. DLS particle size distribution of the biosynthesized TiO2 NPs.

Zeta potential analysis

The measured z-average zeta potential is +17.1 mV (Figure 5) . Having a positive sign does not necessarily mean the particle has good colloidal stability in the measurements conducted, it simply means that it has positive electrophoretic mobility under those conditions. Absence of the secondary DLS intensity mode does not rule out aggregation but is consistent with it. Prior to making a more definitive stability conclusion, the original instrument report should be reviewed to assess for pH, units of conductivity, composition of the dispersant, replicate variance and the quality of the phase signal .

No original zeta-potential instrument export was available, no information on the composition of the dispersant was available, no information on the uncertainty of the conductivity was available, and the result is not independent and is not claimed to be validated.

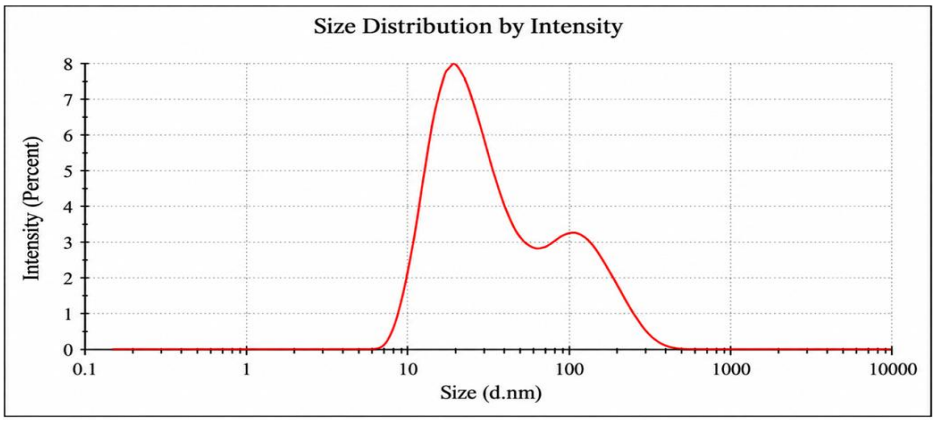


Figure 5. Zeta-potential distribution for mycosynthesized TiO_2 nanoparticles.

Morphological analysis by STEM

The STEM micrographs (Figure 6a–d) reveal variations in particle contrast, shape and apparent aggregation. These observations are qualitative; a representative particle-size distribution can not be reliably determined from the fields displayed in the image alone due to projection effects, over-lap from features in the scene, and image contrast. The provided STEM images cannot be used to report the mean particle diameter, standard deviation, particle count, and size histogram. These must include original calibrated micrographs, a documented selection protocol and measurements of a statistically significant number of well resolved particles.

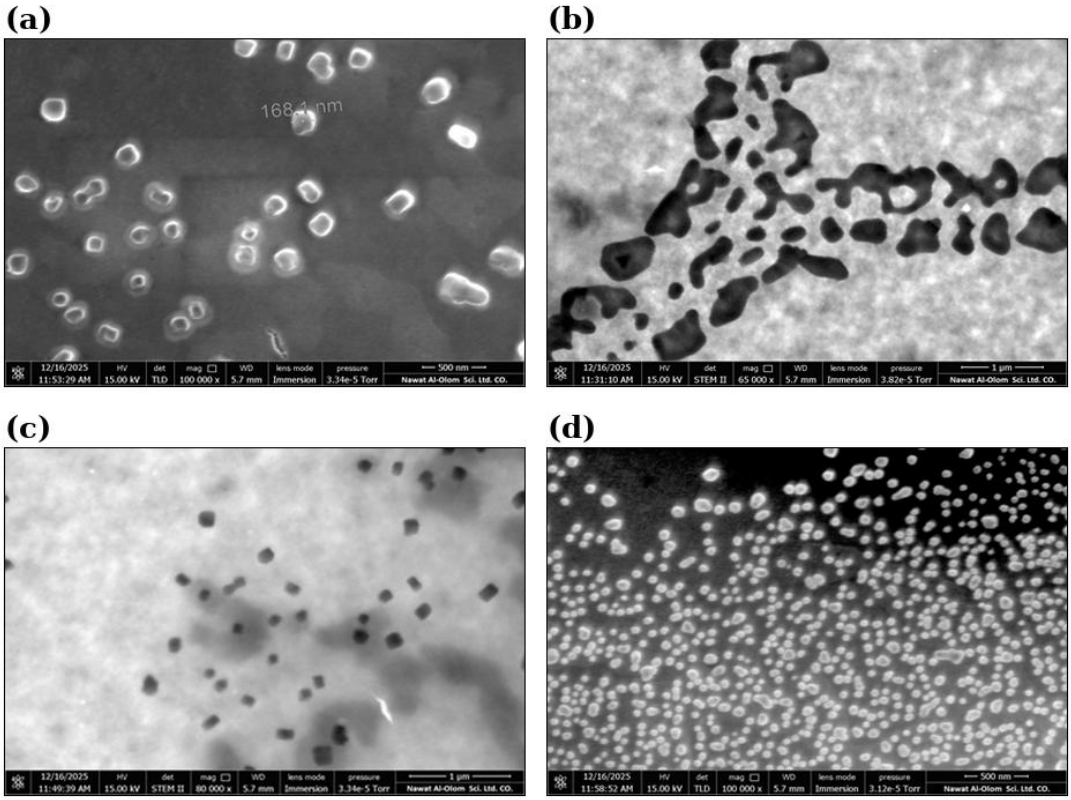


Figure 6. (a–d). Representative STEM micrographs of the prepared material showing high-contrast features and local clustering. Apparent particle outlines and clusters are descriptive observations; specific faceting, crystal habit, and size distributions are not established by these images.

Morphological analysis by high-resolution SEM and hierarchical bulk morphology

The SEM image (Figure 7) reveal that there are also nano scale structures visible on the surface as well as larger agglomerated structures. The previously reported 31.48 nm measurement is for a selected feature, not a representative mean particle diameter statistically representative of all particles. Similarly, the 168.1 nm ring-like feature is a one-time data observation, and should not be compared to the 147.8 nm DLS intensity mode. The numerical agreement between the observations should not be considered as cross method validation as SEM images are performed on dried specimens and DLS measurements are performed in suspension. The magnification series permits a qualitative characterization of nanoscale features in larger aggregates. It does not show a quantitatively resolved hierarchy of primary particles and aggregates, nor prove that the clustering in the dried sample is the result of aggregation in aqueous dispersion.

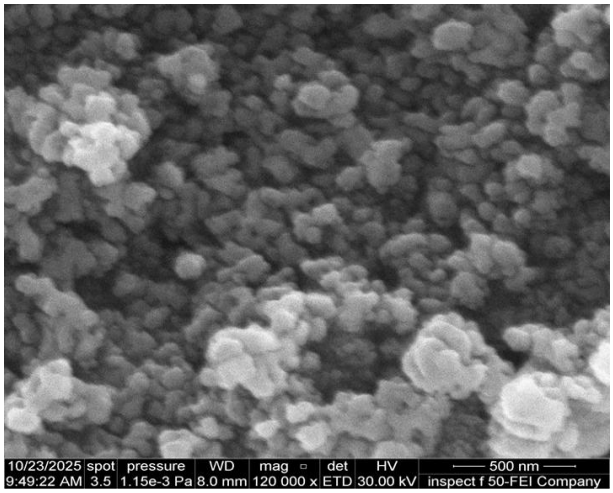


Figure 7. SEM micrographs at different magnifications illustrating heterogeneous surface morphology and regions of clustering in the prepared material. The images do not independently establish a population mean particle size or a quantitative three-level size hierarchy.

Combined, the STEM image and SEM image confirm the morphological heterogeneity and local clustering, but not a validated particle-size mean, histogram, crystal habit nor direct agreement with the DLS.

Antibiotic susceptibility pattern of the clinical *P. aeruginosa* isolates and comparative activity of the TiO_2 NPs

Nine coded *P. aeruginosa* isolates were assessed by agar diffusion (Table 1). These should be consistently identified as the nine rows. The lack of an inhibition zone does not equate to no clinical resistance, however; validated agent-specific interpretive breakpoints should be used to determine this.. For preparation of nanoparticles, a measurable zone would show inhibition under the assay conditions, and will not be considered as clinical susceptibility. This is only a panel of six agents and does not allow classification as MDR/XDR without completing a category based susceptibility assessment. Multidrug-resistant is not a designation of these isolates by this limited zone-diameter panel. In order to confirm MDR and/or XDR status, a standardized antibiotic-class susceptibility profile and known interpretive criteria are required.

Table 1. Inhibition zone diameters (mm) of commercially available antibiotics and mycosynthesized TiO_2 NPs towards clinical isolates of *P. aeruginosa* using the disc diffusion assay

Isolate	CAZ	PRL	MEM	CIP	CN	ATM	TiO_2 NPs
1.	0	0	0	0	0	0	18
2.	0	0	7	0	0	0	20
3.	0	0	0	11	0	0	18
4.	0	0	20	0	0	0	16
5.	0	0	12	0	0	11	15
6.	0	0	0	0	0	17	12
7.	0	0	0	0	0	15	18
8.	0	0	0	0	0	20	18
9.	0	0	11	0	0	14	15
No zone (%)	100.0	100.0	55.6	88.9	100.0	44.4	0.0

Antibiotic disk strengths: CAZ 30 µg; PRL 100 µg; MEM 10 µg; CIP 5 µg; CN 10 µg; ATM 30 µg. Zero = no measurable inhibition zone.

Activity of the six antibiotic discs ranged from measurable zones in all nine isolates (12 mm) to activity in only that one (20 mm) as illustrated in Figure 8 . This observation suggests in-vitro inhibition rather than effect on all species of bacteria. Diffusion and loading differences between a nanoparticle

suspension and antibiotic discs make it unfeasible to make potency comparisons between the two using disc diffusion diameters.

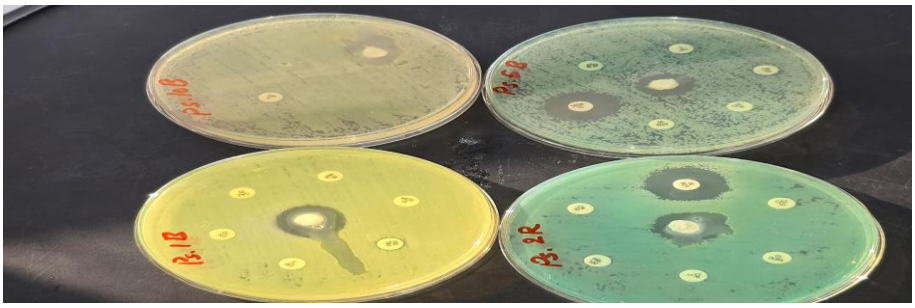


Figure 8. The antibacterial activity of TiO_2NPS and 9 selected antibiotices against *P.aeruginosa* isolates.

In previous studies, it has been suggested that TiO_2 materials exert their action through mechanisms such as oxidative stress, cell-envelope interactions and others, but this experiment did not quantify the concentration of reactive oxygen species, membrane damage, the effects if lighting or the uptake of the nanoparticles. Thus, the mode of inhibition is still not known. The results should not be taken as proof that the preparation bypasses all resistance mechanisms to the antibiotics. Figure 9 summarizes the number of isolates with a measurable zone: TiO_2 preparation 9/9, meropenem 4/9, ciprofloxacin 1/9 and aztreonam 5/9.

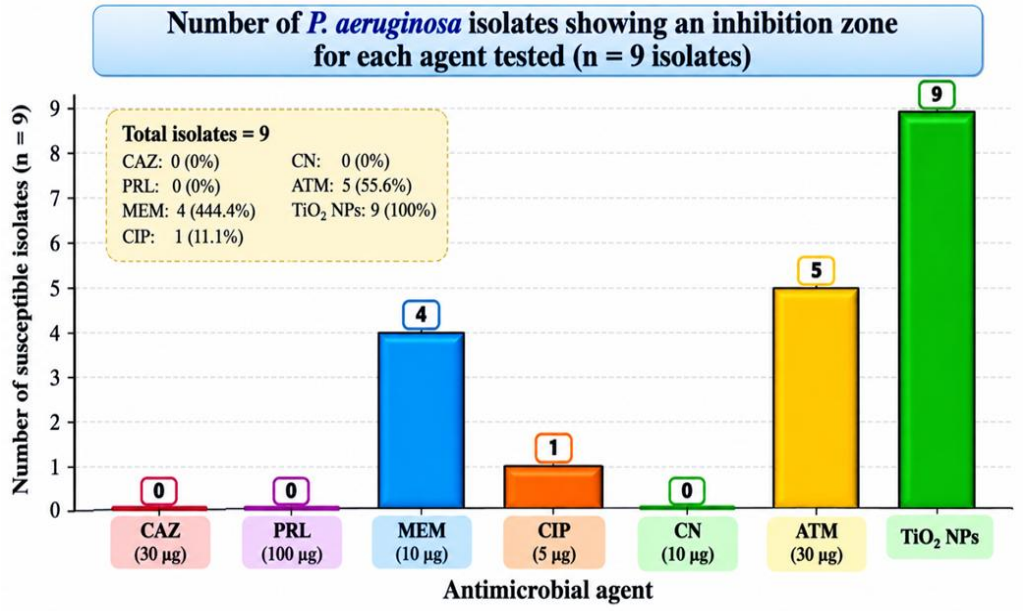


Figure 9. summarizes the number of isolates with a measurable zone: TiO_2 preparation 9/9, meropenem 4/9, ciprofloxacin 1/9 and aztreonam 5/9, with no measurable zones for the other three antibiotic discs. This is a descriptive comparison of agar diffusion outcomes and does not establish superior clinical efficacy or equivalent dose-normalized potency. .

Minimum inhibitory concentration (MIC) of the TiO2 NPs and meropenem

Nine isolates had MICs recorded for TiO_2 nanoparticles ranging from 50 to 100 µg/mL with a descriptive mean value of 72.2 µg/mL (Table 2). The method available is broth dilution and not a validated microplate based microdilution assay. If turbidity or OD600 is used to determine MIC, an assay control should be taken into consideration due to the contribution of optical scattering by suspended nanoparticles. Because meropenem MIC data are only available for two isolates, the two agents cannot be compared on the entire isolate panel based on these data.

Table 2. MIC (µg/mL) of the mycosynthesized TiO_2 nanoparticles and meropenem for the studied *Pseudomonas aeruginosa* isolates

Isolate / Statistic	TiO_2 NPs MIC (µg/mL)	Meropenem MIC (µg/mL)
1	100	50
2	50	25
3	50	—
4	100	—
5	100	—
6	50	—
7	100	—
8	50	—
9	50	—
Mean ± SD	72.22 ± 26.35	37.50 ± 17.68
Median	50	37.50
Range	50–100	25–50
Valid observations (n)	9	2

Note. Values are reported in µg/mL. SD is the sample standard deviation. A dash (—) indicates an unavailable measurement, not a zero MIC or confirmed resistance. Descriptive statistics are based on available observations only.

Recorded nanoparticle MICs were 50 µg/mL for numeric isolates 2, 3, 6, 8, and 9 and 100 µg/mL for isolates 1, 4, 5, and 7 (n = 9; descriptive mean ± sample SD = 72.2 ± 26.4 µg/mL). These figures are a summary of the numbers in Table 2 and are not analytical precision or statistical significance. The recorded MIC of 50 µg/mL for numeric isolate 8 is provisional, as extensive growth after subculture is noted in Table 3 at 200 µg/mL which needs to be reviewed in the light of raw observations and repeated viability-based testing .

The MIC of meropenem was available for numeric isolates 1 and 2 (50 µg/mL and 25 µg/mL, respectively, n = 2), whereas the MIC of meropenem (reported) was 100 and 50 µg/mL for those same numeric IDs. The inconsistent and incomplete measurements cannot justify a potency ranking or superiority claims. There are also differences between disc diffusion and broth MIC results, in terms of the endpoint of the assay.

Minimum bactericidal concentration (MBC) of the TiO_2NPs and meropenem

The selected broth concentrations at or above the reported MIC were subcultured in BHI agar by transferring 100 µL of the broth culture, and the subcultures were investigated after 24 h. The results of the growth/no growth testing are recorded in Table 3. It is only where the experimental definition and reduction in number of live cells are well documented that an MBC may be assigned and a formal bactericidal ratio obtained from a no-growth observation at one concentration.

The records for the isolates treated with nanoparticles show no colonies at 200, 100 and 200 µg/mL, respectively. This is a demonstration of no measurable growth under the plating conditions specified and not a quantitative demonstration of bactericidal endpoint. Isolates 3, 7 and 8 continued to grow and no subculture results were provided for isolates 4, 6 and 9. The other isolates (1 and 2) grown on reculture at reported concentrations were also meropenem-treated. Therefore, these data will not be used to determine formal MIC values or bactericidal/bacteriostatic labels for isolate 8, as there is significant viable growth on subculture at 200 µg/mL that is in conflict with the OD based MIC. This difference does not imply that there is a specific optical interference mechanism, but rather that the MIC needs to be verified. Recommended: repeat assays using particle only blanks, standardized inocula and independent viable count endpoints.

Table 3. The results of the growth/no growth testing are recorded

Isolate	Agent	MIC (µg/mL)	Subculture outcome	MBC (µg/mL)	MBC/MIC	Interpretation
1	TiO_2 NPs	100	No growth at 200	No growth at tested concentration*	Not established	No growth on subculture; formal MBC unverified
1	Meropenem	50	Heavy confluent growth at 100 and 200	Not established	—	Growth observed; MBC not established
2	TiO_2 NPs	50	No growth at 100	No growth at tested concentration*	Not established	No growth on subculture; formal MBC unverified
2	Meropenem	25	Colonies present at 100 and 200	Not established	—	Growth observed; MBC not established
3	TiO_2 NPs	50	Residual colonies (3–4) at 100	Not established	—	Growth observed; MBC not established
5	TiO_2 NPs	100	No growth at 200	No growth at tested concentration*	Not established	No growth on subculture; formal MBC unverified
7	TiO_2 NPs	100	Residual colonies at 200	Not established	—	Growth observed; MBC not established
8	TiO_2 NPs	50	Extensive growth at 200	Not determined	—	See limitation (Section 3.9)
4, 6, 9	—	—	Not subcultured	Not determined	—	Outside the scope of this experiment

Notes: No growth at tested concentration reports the observed subculture result only; it is not a validated MBC determination. MBC/MIC ratios cannot be calculated without established MBC values. A dash (—) indicates unavailable or inapplicable data. Concentrations are expressed in µg/mL.*

A provisional optical MIC of 50 µg/mL has been reported and is provisional and the value should not be used as a confirmed MIC (optical) for isolate 8 until independent confirmation of viability is available.

The evidence does not support observation of subculture of isolates 3, 4 or 6 which are no-growth conditions. The bactericidal classification should not be made from a visually negative plate only and should be done using a validated quantitative viable criterion. No data are found for bactericidal activity for all nine isolates or clinical superiority over meropenem.

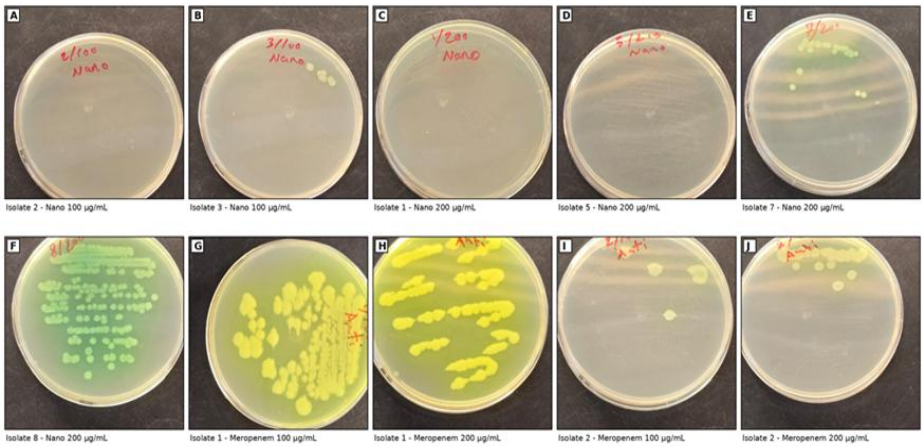


Figure 9. MBC agar subculture plates : TiO2NPS and Meropenem against *P. aeruginosa* isolates.

Structure activity relationships and translational considerations

The in-vitro inhibition results require further investigation and are not able to suggest a structure–activity mechanism. The physical characteristics, such as crystalline phase, particle-size distribution and dispersion stability, ROS production and cytotoxicity are still insufficiently characterized.

Problems that remain to be addressed in the future are combination therapy and antibiofilm performance and clinical translation, which are not measured here.

LIMITATIONS

Limitations include: (1) No validated image-based particle-size distribution and particle count for SEM/STEM; (2) No complete instrument metadata or replicate distributions or distribution sensitivity to dispersion conditions; (3) No complete or consistent antibiotic-category data for formal assignment of MDR/XDR phenotype; (4) No complete or confirmatory phase/elemental analysis (EDX/XPS); (5) No complete or confirmatory raw XRD export; (6) No direct ROS/dark-versus-illumination assay; (7) No confirmed or validated cytotoxicity, biofilm or in-vivo testing; (8) No confirmed or validated particle count for broth assay; (9) No confirmed or validated phase/elemental analysis (EDX/XPS) for broth assay; and (10) No nanoparticle-only blanks for broth assay. The small number of isolates in the panel restricts generalizability.

CONCLUSION

The preparation prepared with the Aspergillus niger cell-free filtrate exhibited measurable agar inhibition zones (12–20 mm) against all nine isolates of P. aeruginosa tested. The reported MICs ranged from 50 to 100 µg/mL, with the possibility of optical interference being caused by the nanoparticles not ruled out. Isolates 1, 2 and 5 were not observed to grow in subculture, although a quantitative bactericidal endpoint was not determined. XRD showed scattering without any possible anatase/rutile indexing, while DLS showed a Z-average diameter of 28.38 nm (PdI 0.383) and a zeta potential of +17.1 mV. Qualitative morphology was supported by using microscopy, but no particle size distribution was achieved.

REFERENCES

1. Abdelkader, D. H., Negm, W. A., Elekhnawy, E., Eliwa, D., Aldosari, B. N., & Almurshedi, A. S. (2022). Zinc oxide nanoparticles as potential delivery carrier: green synthesis by Aspergillus niger endophytic fungus, characterization, and in vitro/in vivo antibacterial activity. Pharmaceuticals, 15(9), 1057.
2. Ahmad, W., Jaiswal, K. K., & Soni, S. (2020). Green synthesis of titanium dioxide (TiO2) nanoparticles by using Mentha arvensis leaves extract and its antimicrobial properties. Inorganic and Nano-Metal Chemistry, 50(10), 1032–1038.
3. Ahmed, F. Y., Farghaly Aly, U., Abd El-Baky, R. M., & Waly, N. G. F. M. (2020). Comparative study of antibacterial effects of titanium dioxide nanoparticles alone and in combination with antibiotics on MDR Pseudomonas aeruginosa strains. International Journal of Nanomedicine, 3393–3404.
4. Alavi, M., Kahrizi, D., Martinez, F., & Rai, M. (2023). Nanomaterials to combat pathogenic microorganisms. In Frontiers in Microbiology (Vol. 14, p. 1160196). Frontiers Media SA.
5. Alcazar, K., Tous, L., Herrera, A., Martinez-Bernett, D., & Saba, M. (2026). TiO2 Nanoparticles obtained by green synthesis: characterization and evaluation of their effect on the self-cleaning and antifungal properties of an aqueous paint-type coating. Nanomaterials, 16(2), 91.
6. Alhosani, F., Islayem, D., Almansoori, S., Zaka, A., Nayfeh, L., Rezk, A., Yousef, A. F., Pappa, A. M., & Nayfeh, A. (2025). Antibiofilm activity of ZnO–Ag nanoparticles against Pseudomonas aeruginosa. Scientific Reports, 15(1), 17321.
7. Arora, B., Murar, M., & Dhumale, V. (2015). Antimicrobial potential of TiO2 nanoparticles against MDR Pseudomonas aeruginosa. Journal of Experimental Nanoscience, 10(11), 819–827.
8. Babayevska, N., Przysiecka, Ł., Iatsunskyi, I., Nowaczyk, G., Jarek, M., Janiszewska, E., & Jurga, S. (2022). ZnO size and shape effect on antibacterial activity and cytotoxicity profile. Scientific Reports, 12(1), 8148.
9. Bhattacharjee, S. (2016). DLS and zeta potential–what they are and what they are not? Journal of Controlled Release, 235, 337–351.

10. Bishoyi, A. K., Sahoo, C. R., Samal, P., Mishra, N. P., Jali, B. R., Khan, M. S., & Padhy, R. N. (2024). Unveiling the antibacterial and antifungal potential of biosynthesized silver nanoparticles from Chromolaena odorata leaves. Scientific Reports, 14(1), 7513.
11. Canchanya-Huaman, Y., Mayta-Armas, A. F., Pomalaya-Velasco, J., Bendezú-Roca, Y., Guerra, J. A., & Ramos-Guivar, J. A. (2021). Strain and grain size determination of CeO2 and TiO2 nanoparticles: comparing integral breadth methods versus rietveld, μ-Raman, and TEM. Nanomaterials, 11(9), 2311.
12. Carvalho, P. M., Felício, M. R., Santos, N. C., Gonçalves, S., & Domingues, M. M. (2018). Application of light scattering techniques to nanoparticle characterization and development. Frontiers in Chemistry, 6, 237.
13. Chen, H.-S., Su, C., Chen, J.-L., Yang, T.-Y., Hsu, N.-M., & Li, W.-R. (2011). Preparation and Characterization of Pure Rutile TiO2 Nanoparticles for Photocatalytic Study and Thin Films for Dye-Sensitized Solar Cells. Journal of Nanomaterials, 2011(1), 869618.
14. Darwesh, H., Abdalla, M., Goevert, D., & Hamzah, H. (2026). Bacterial synthesis parameters and antibacterial mechanisms of titanium dioxide nanoparticles against multidrug resistant Gram-negative pathogens. Discover Applied Sciences.
15. Dias, M. A. M., & Nitschke, M. (2023). Bacterial-derived surfactants: an update on general aspects and forthcoming applications. Brazilian Journal of Microbiology, 54(1), 103–123.
16. Donkor, G. Y., & Dahl, J.-U. (2026). Implications of bacterial exposure to reactive oxygen and chlorine species. Infection and Immunity, e00010-23.
17. Dreno, B., Alexis, A., Chuberre, B., & Marinovich, M. (2019). Safety of titanium dioxide nanoparticles in cosmetics. Journal of the European Academy of Dermatology and Venereology, 33, 34–46.
18. El Menofy, N. G., Tawfick, M. M., & Badawy, M. S. E. M. (2025). Molecular study of carbapenem-resistant Pseudomonas aeruginosa causing wound infection in an Egyptian tertiary hospital. The Journal of Infection in Developing Countries, 19(07), 997–1006.
19. Flockton, T. R., Schnorbus, L., Araujo, A., Adams, J., Hammel, M., & Perez, L. J. (2019). Inhibition of Pseudomonas aeruginosa biofilm formation with surface modified polymeric nanoparticles. Pathogens, 8(2), 55.
20. Flores-Treviño, S. (2025). Antimicrobial resistance and hospital-and community-associated infections. In Antibiotics (Vol. 14, Issue 5, p. 514). MDPI.
21. Fontoura, I., Veriato, T. S., Raniero, L. J., & Castilho, M. L. (2023). Analysis of capped silver nanoparticles combined with imipenem against different susceptibility profiles of Klebsiella pneumoniae. Antibiotics, 12(3), 535.
22. Hamid, D. K. A. El, Desouky, E. M., Ellatif, S. A., Abed, N. N., & Mahfouz, A. Y. (2025). Biofabrication of TiO2 nanoparticles via Aspergillus niger DS22 supernatant: bioreactor optimization and multi-activity profiling. Biomass Conversion and Biorefinery, 15(5), 7663–7686.
23. Hetta, H. F., Ramadan, Y. N., Al-Harbi, A. I., A. Ahmed, E., Battah, B., Abd Ellah, N. H., Zanetti, S., & Donadu, M. G. (2023). Nanotechnology as a promising approach to combat multidrug resistant bacteria: a comprehensive review and future perspectives. Biomedicines, 11(2), 413.
24. Jávorfi, T. (2022). Advances and applications in structural approaches.
25. Khan, F., Manivasagan, P., Lee, J.-W., Pham, D. T. N., Oh, J., & Kim, Y.-M. (2019). Fucoidan-stabilized gold nanoparticle-mediated biofilm inhibition, attenuation of virulence and motility properties in Pseudomonas aeruginosa PAO1. Marine Drugs, 17(4), 208.
26. Malawong, S., Thammawithan, S., Sirithongsuk, P., Daduang, S., Klaynongsruang, S., Wong, P. T., & Patramanon, R. (2021). Silver nanoparticles enhance antimicrobial efficacy of antibiotics and restore that efficacy against the melioidosis pathogen. Antibiotics, 10(7), 839.
27. Mishra, R. C., Kalra, R., Dilawari, R., Goel, M., & Barrow, C. J. (2022). Bio-synthesis of Aspergillus terreus mediated gold nanoparticle: antimicrobial, antioxidant, antifungal and in vitro cytotoxicity studies. Materials, 15(11), 3877.

28. Nabi, G., Anjum, T., Aftab, Z., Rizwana, H., & Akram, W. (2024). TiO2 nanoparticles: Green synthesis and their role in lessening the damage of Colletotrichum graminicola in sorghum. Food Science & Nutrition, 12(10), 7379–7391.
29. Nagaraj, G., Brundha, D., Chandraleka, C., Arulpriya, M., Kowsalya, V., Sangavi, S., Jayalakshmi, R., Tamilarasu, S., & Murugan, R. (2020). Facile synthesis of improved anatase TiO2 nanoparticles for enhanced solar-light driven photocatalyst: G. Nagaraj et al. SN Applied Sciences, 2(4), 734.
30. Nakazato, G., & Kobayashi, R. K. T. (2022). Nanotechnology for Antimicrobials, Volume 2. In Frontiers in Microbiology (Vol. 13, p. 860908). Frontiers Media SA.
31. Newman, M. D. M. D., Stotland, M. D. M., & Ellis, M. D. J. I. (2009). The safety of nanosized particles in titanium dioxide–and zinc oxide–based sunscreens. Journal of the American Academy of Dermatology, 61(4), 685–692.
32. Pal, S., Tak, Y. K., & Song, J. M. (2007). Does the antibacterial activity of silver nanoparticles depend on the shape of the nanoparticle? A study of the gram-negative bacterium Escherichia coli. Applied and Environmental Microbiology, 73(6), 1712–1720.
33. Pham, D. T. N., Khan, F., Phan, T. T. V., Park, S., Manivasagan, P., Oh, J., & Kim, Y.-M. (2019). Biofilm inhibition, modulation of virulence and motility properties by FeOOH nanoparticle in Pseudomonas aeruginosa. Brazilian Journal of Microbiology, 50(3), 791–805.
34. Rajakumar, G., Rahuman, A. A., Roopan, S. M., Khanna, V. G., Elango, G., Kamaraj, C., Zahir, A. A., & Velayutham, K. (2012). Fungus-mediated biosynthesis and characterization of TiO2 nanoparticles and their activity against pathogenic bacteria. Spectrochimica Acta Part A: Molecular and Biomolecular Spectroscopy, 91, 23–29.
35. Reyes-Coronado, D., Rodríguez-Gattorno, G., Espinosa-Pesqueira, M. E., Cab, C., de Coss, R., & Oskam, G. (2008). Phase-pure TiO2 nanoparticles: anatase, brookite and rutile. Nanotechnology, 19(14), 145605.
36. Rodríguez-Martínez, J.-M., Poirel, L., & Nordmann, P. (2009). Molecular epidemiology and mechanisms of carbapenem resistance in Pseudomonas aeruginosa. Antimicrobial Agents and Chemotherapy, 53(11), 4783–4788.
37. Sahithya, K., Ekanayake, A. K., Hemanathan, D., Sindhu, R., & Jaswanth, B. (2024). Mycosynthesis of CuO Nanoparticles Using Aspergillus niger and Their Bioefficiency against Human Pathogens. Nano Biomedicine & Engineering, 16(2), 264.
38. Saied, E., Abdel-Maksoud, M. A., Alfuraydi, A. A., Kiani, B. H., Bassyouni, M., Al-Qabandi, O. A., Bougafa, F. H. E., Badawy, M. S. E. M., & Hashem, A. H. (2024). Endophytic Aspergillus hiratsukae mediated biosynthesis of silver nanoparticles and their antimicrobial and photocatalytic activities. Frontiers in Microbiology, 15, 1345423.
39. Sanches, P. L., Geaquinto, L. R. de O., Cruz, R., Schuck, D. C., Lorencini, M., Granjeiro, J. M., & Ribeiro, A. R. L. (2020). Toxicity evaluation of TiO2 nanoparticles on the 3D skin model: a systematic review. Frontiers in Bioengineering and Biotechnology, 8, 575.
40. Sati, H., Carrara, E., Savoldi, A., Hansen, P., Garlasco, J., Campagnaro, E., Boccia, S., Castillo-Polo, J. A., Magrini, E., & Garcia-Vello, P. (2025). The WHO Bacterial Priority Pathogens List 2024: a prioritisation study to guide research, development, and public health strategies against antimicrobial resistance. The Lancet Infectious Diseases, 25(9), 1033–1043.
41. Siddiqi, K. S., & Husen, A. (2016). Fabrication of metal nanoparticles from fungi and metal salts: scope and application. Nanoscale Research Letters, 11(1), 98.
42. Sidhu, A. K., Verma, N., & Kaushal, P. (2022). Role of biogenic capping agents in the synthesis of metallic nanoparticles and evaluation of their therapeutic potential. Frontiers in Nanotechnology, 3, 801620.
43. Slavin, Y. N., Asnis, J., Häfeli, U. O., & Bach, H. (2017). Metal nanoparticles: understanding the mechanisms behind antibacterial activity. Journal of Nanobiotechnology, 15(1), 65.
44. Smekalova, M., Aragon, V., Panacek, A., Prucek, R., Zboril, R., & Kvitek, L. (2016). Enhanced antibacterial effect of antibiotics in combination with silver nanoparticles against animal pathogens. The Veterinary Journal, 209, 174–179.

45. Soares, A. R., Pavoski, G., Espinosa, D. C. R., Yin, W., & dos Passos Galluzzi Baltazar, M. (2026). Current challenges and future directions in the green synthesis of nanoparticles using fungi. Bioprocess and Biosystems Engineering, 1–26.
46. Somvanshi, S. B., Kharat, P. B., Khedkar, M. V, & Jadhav, K. M. (2020). Hydrophobic to hydrophilic surface transformation of nano-scale zinc ferrite via oleic acid coating: magnetic hyperthermia study towards biomedical applications. Ceramics International, 46(6), 7642–7653.
47. Van Driessche, A. E. S., Van Gerven, N., Joosten, R. R. M., Ling, W. L., Bacia, M., Sommerdijk, N., & Sleutel, M. (2021). Nucleation of protein mesocrystals via oriented attachment. Nature Communications, 12(1), 3902.
48. Wei, L., Zhang, Q., Xie, A., Xiao, Y., Guo, K., Mu, S., Xie, Y., Li, Z., & He, T. (2022). Isolation of bioactive compounds, antibacterial activity, and action mechanism of spore powder from Aspergillus niger xj. Frontiers in Microbiology, 13, 934857.
49. Xie, X., Liu, Z., Huang, J., Wang, X., Tian, Y., Xu, P., & Zheng, G. (2024). Molecular epidemiology and carbapenem resistance mechanisms of Pseudomonas aeruginosa isolated from a hospital in Fujian, China. Frontiers in Microbiology, 15, 1431154.
50. Yadav, S., Pawar, S., Patil, S., & Yadav, S. A. (2025). Inhibition of Pseudomonas aeruginosa Biofilm Formation Using Silver Nanoparticles. Cureus, 17(1.(
51. Yoon, Y. K., Sung, Y. H., Kim, J. Y., & Sohn, J. W. (2026). P-1294. Epidemiology of Carbapenem-resistance Mechanisms and the Utility of Newly Introduced Beta-lactams/beta-lactam Inhibitors in Patients with Pseudomonas aeruginosa Bacteremia. Open Forum Infectious Diseases, 13(Supplement_1), ofaf695-1482.
52. Yu, Z., Li, Q., Wang, J., Yu, Y., Wang, Y., Zhou, Q., & Li, P. (2020). Reactive oxygen species-related nanoparticle toxicity in the biomedical field. Nanoscale Research Letters, 15(1), 115.
53. Yuan, Q., Guo, L., Li, B., Zhang, S., Feng, H., Zhang, Y., Yu, M., Hu, H., Chen, H., & Yang, Q. (2023). Risk factors and outcomes of inpatients with carbapenem-resistant Pseudomonas aeruginosa bloodstream infections in China: a 9-year trend and multicenter cohort study. Frontiers in Microbiology, 14, 1137811.

النشاط المضاد للبكتيريا لجسيمات ثاني أكسيد التيتانيوم النانوية المُحضّرة بواسطة فطر الرشاشية السوداء ضد عزلات سريرية من بكتيريا الزائفة الزنجارية

الملخص

تُعدّ الزائفة الزنجارية بكتيريا مقاومة للأدوية المتعددة، ما يُمثّل تحديًا علاجيًا كبيرًا. في هذه الدراسة، استُخدم مُرشّح خالٍ من الخلايا لفطر الرشاشية السوداء كمصدر لتحضير جسيمات ثاني أكسيد التيتانيوم النانوية، واختُبرت فعاليتها ضد 9 عزلات سريرية من الزائفة الزنجارية. استُخدمت تقنيات حيود الأشعة السينية (XRD)، ومطيافية الأشعة تحت الحمراء بتحويل فورييه (FTIR)، وتشتت الضوء الديناميكي (DLS)، وتحليل جهد زيتا، والمجهر الإلكتروني الماسح النافذ (STEM)، والمجهر الإلكتروني الماسح (SEM) للتحليل الفيزيائي والكيميائي. أظهر مخطط حيود الأشعة السينية انعكاسًا واسعًا مُنتشرًا حول 23.5° (θ2)، ولكن لم تكن الانعكاسات كافية لتمييز الأناتاز والروتيل. أظهرت نتائج قياس تشتت الضوء الديناميكي (DLS) متوسط قطر هيدروديناميكي قدره 28.38 نانومتر (PdI 0.383)، ولكن تم الحصول على ذروتي شدة عند 27.70 و147.8 نانومتر، وهما غير قابلتين للمقارنة المباشرة مع أبعاد الحالة الجافة المقاسة بواسطة المجهر الإلكتروني الماسح (SEM). بلغ جهد زيتا المُبلغ عنه +17.1 ملي فولت، مما يشير إلى استقرار كهروستاتيكي ضئيل في ظل الظروف المذكورة. بعد التعرض للجسيمات النانوية، تم تثبيط نمو جميع العزلات التسع، كما يتضح من وجود مناطق تثبيط قابلة للقياس (12-20 مم)، وتراوح الحد الأدنى للتركيز المثبط (MIC) من 50 إلى 100 ميكروغرام/مل. لم تُظهر النتائج أي نمو للمزارع الفرعية عند التركيز المختبر للعزلات 1 و2 و5، بينما لم يتم تحقيق نقاط النهاية القاتلة للبكتيريا للعزلات الأخرى. تشير هذه النتائج المخبرية إلى ضرورة إجراء المزيد من الدراسات حول هذا المستحضر كمضاد للبكتيريا، ولكنها لا تُثبت فعاليته كمضاد للبكتيريا بشكل قاطع، أو آلية عمله، أو فعاليته السريرية.

الكلمات المفتاحية: التخليق الأخضر؛ الرشاشية السوداء؛ جسيمات ثاني أكسيد التيتانيوم النانوية؛ مقاومة متعددة للأدوية؛ الزائفة الزنجارية؛ الحد الأدنى للتركيز المثبط؛ الحد الأدنى للتركيز القاتل للبكتيريا.